1   Supplemental material

2   *1. Detailed methods*

3   *1.1 Sediment analyses*

4   Sediment samples were obtained from archived DSDP, ODP, and piston cores from the

5   Lamont-Doherty Earth Observatory (LDEO) core archive. Samples were dried at 50 °C, and

6   sediment aliquots for Total Organic C (TOC) analysis were acidified using 1 N HCl for at least

7   12 hours or until effervescence ceased. Following acidification, samples were centrifuged and

8   washed 3x with DI water and re-dried before homogenization with an agate mortar and pestle.

9   Approximately 100 mg was combusted with Cu/CuO_x in an evacuated quartz tube at 910 °C

10   overnight. Resulting CO_2 was purified and collected on a gas line. Sample aliquots for

11   carbonate analysis were acidified with 100% phosphoric acid at 70 °C in a Finnigan Gas Bench

12   CO_2 handling system. For all samples, CO_2 was quantified using manometry, and all isotope

13   measurements were conducted on a Finnigan MAT 252 mass spectrometer operated in dual inlet

14   mode. All $\delta^{13}C$ values are reported relative to VPDB C isotope standard. For measurements of

15   C isotopic composition of carbonate within Altered Oceanic Crust (AOC), we used a microdrill

16   to obtain samples of the carbonate veins and breccia matrix. These samples were then analyzed

17   in an identical fashion to sedimentary C.

18

19   *1.2 Sediment and unit thicknesses*

20   Archived 3.5 kHz single channel seismic lines from the Lamont-Doherty Earth

21   Observatory (LDEO) collection were used to determine overall sediment thickness and the

22   thicknesses of geochemically distinct units outboard of the Sunda margin. Archived profiles

23   from the following cruise tracks were used:

24   • RC 1107

25   • RC 1402

26   • RC 1403

27   • V 1909

28   • V 2009

29   • V 2410

30   • V 2819

31   • V 2901

32   • V 3503

33   • V 3616

34   Seafloor, basement, and unit boundary picks, made using the GeoMap App program for these

35   profiles, were augmented with additional constraints from more recent published multichannel

36   lines (Kopp and Kukowski, 2003; Lüschen et al., 2011; Kopp et al., 2006; Planert et al., 2010;

37   Kopp, 2013; Kopp et al., 2009; McNeill et al., 2016; Dean et al., 2010). Geochemical unit

38   boundaries (Nicobar Fan, terrigenous trenchfill, pelagic material, and calcareous turbidites) were

39   defined by picks following the seismic interpretations in the Initial Report volumes of the

40   appropriate DSDP/ODP sites and subsequent seismic studies. The terrigenous trenchfill unit is

41   defined by reflectors that converge moving away from the trench, and the top of the Nicobar Fan

42   was inferred to coincide with the base of this unit as reported elsewhere (e.g. Dean et al., 2010).

43   The base of the Nicobar Fan lacks clear seismic reflectors, and as such, we assumed a uniform

44   thickness of 200 m for the underlying pelagic unit (which is intermediate between results from

45   DSDP 211 and IODP 1480) rather than using dubious seismic picks to constrain the thickness of

46   the Nicobar Fan unit (Expedition 22 Scientific Party, 1974; McNeill et al., 2017). The lower

47   extent of the unit of calcareous turbidites from the Exmouth Plateau/Australian margin is defined

48   by a distinct set of reflectors (Ludden and Gradstein, 1990), and since this unit is uppermost at

49   Sites 261 and 765 where it is sampled, we infer that overlying sediment is likely to be

50   quantitatively minimal throughout the margin. Therefore, constraining this unit's thickness – as

51   well as that of the underlying pelagic sediments – was straightforward. The lack of a clear

52   seismic boundary between the calcareous turbidite unit and the trenchfill wedge in seismic

53   profiles along the southeastern portion of the margin led us to assign a thickness for the trenchfill

54   unit by subtracting the thickness of the other units outboard of the trench from the overall

55   sediment thickness at the trench. This approach, while necessary to constrain overall sediment

56   flux to the trench, is unlikely to substantially affect our estimates of subducting C because the

57   entirety of the trench wedge appears to be off-scraped through much of the margin. While the

58   Roo Rise is inducing localized subduction erosion along eastern Java, sediment cover on the rise

59   is minimal, and sediments trenchward of it are difficult to interpret from seismic profiles.

60   Indeed, East Java stands out as a region of low sediment cover (Figures DR2 and DR3), so while

61   our estimates consider the subduction of the thin sediment veneer currently present, significantly

62   more sediment and sedimentary C may have subducted in the recent past when the Roo Rise first

63   impinged upon the margin.

64   When seismic velocity profiles reported two-way travel time rather than sediment

65   thickness and sediment velocity models were not available, sediment velocities of 2 and 2.5 km/s

66   were used to construct upper and lower bounds on sediment thickness respectively. While these

67   velocities are greater than those determined for surficial sediments (Dean et al., 2010), they

68   encapsulate the range of velocities expected for the deeper sediments that escape off-scraping at

69   the deformation front along much of the margin. Therefore, these seismic velocity bounds are

70   reasonable for estimating subducting C flux and may slightly overestimate the amount of

71   sediment – and hence C – present at the trench. A total of ~8000 picks were made, and

72   additional unit and sediment thickness constraints from DSDP Sites 211, 213, 260, 261, ODP

73   Site 765, and IODP Site 1480 were also incorporated. Using these data, surfaces were

74   constructed to model unit and overall sediment thicknesses and extrapolate these from core sites

75   to the trench. With these models and results from sediment analyses, we estimated the amount

76   and types of C within the sediment column at the trench.

77   Plate motion models of the Indoaustralian plate relative to the stable Sunda core from

78   McNeill et al. (2014) were used to convert C content into a C flux to the trench, calculated at

79   points along the trench that correspond to the MORVEL plate boundary between the

80   Indoaustralian and Sunda plates (Argus et al., 2011). Single and multichannel seismic profiles

81   as well as velocity models across the trench (Lüschen et al., 2011; Kopp et al., 2009, 2006; Kopp

82   and Kukowski, 2003; Kopp et al., 2001; Planert et al., 2010) were used to estimate the fraction of

83   the overall sediment and C flux bypassing the deformation front and subducting past ~20 km, the

84   maximum seismically-resolved depth. These estimates were combined with those from McNeill

85   et al. (2014) to generate upper and lower bounds on the sediment subducting past the

86   deformation front. This range in possible subduction channel thickness leads to the range in

87   estimates for subducted C amount.

88

89   *2. Comparing shipboard and shore-based organic C analyses*

90   The tendency for disagreement between shipboard estimates of Total Organic C (TOC)

91   made during coring expeditions and shorebased measurements has been previously documented

92   (Olivarez Lyle and Lyle, 2006). Shipboard TOC is typically not measured directly but calculated

93   as the difference between total C (measured by combustion elemental analysis) and carbonate C

94   (measured by coulometry). However, this method can lead to substantial uncertainty. Several

95   hundred replicate shipboard analyses conducted on a total of 5 samples from IODP Site 1480

96   give one-sigma uncertainties of 35 to 180% (McNeill et al., 2017). Furthermore, comparing the

97   pool of shipboard data from DSDP Sites 211, 260, 261, 262, and ODP Site 765 (Ludden and

98   Gradstein, 1990; Plank and Ludden, 1992; Bode, 1974; Pimm, 1974) with our shore-based TOC

99   results shows that we are unable to reproduce the highest shipboard TOC values and that the

100   distribution of values is substantially different between ship- and shore-based analyses (Figure

101   DR1). While these analyses were not conducted on precisely the same samples, the large

102   number of data compiled suggests a true difference between the two distributions, and indeed a

103   one-tailed non-parametric unpaired t-test reveals that the mean of shipboard data is higher than

104   that of shorebased data at a statistically significant level ($p < 10^{-10}$). This suggests that using

105   shipboard data is likely to overestimate of the abundance of organic C and to overemphasize its

106   importance in C-cycling. Future studies of organic C cycling at convergent margins should

107   therefore rely on shorebased reanalysis of shipboard samples.

108

109   *3. Caveats in determining provenance of arc* CO_2

110   The three endmember mixing model of Sano and Marty (1995) has been used previously

111   to establish the provenance of volcanic and hydrothermal CO_2 released along Indonesia

112   (Halldórsson et al., 2013; Figure DR3). In this model, the $\delta^{13}C$ and $CO_2/^3He$ composition of

113   volcano or hydrothermal CO_2 are used to resolve contributions from subducting carbonate and

114   organic C as well as C from the mantle wedge. While the $\delta^{13}C$ of organic C can be readily

115   measured, the meaning of a $CO_2/^3He$ ratio for organic C is less clear. A value of $\sim10^{14}$ is

116   typically used for this ratio, as well as for the $CO_2/^3He$ ratio of sedimentary carbonate (termed

117   "limestone" in previous work; Marty et al., 1989; Hilton et al., 2002; Halldórsson et al., 2013).

118   Because typical volcanic gases have a $CO_2/^3He$ ratio of $\sim10^{10}$, CO_2 provenance results from this

119   mixing model are relatively insensitive to changes in these endmember compositions. However,

120   the $CO_2/^3He$ composition of the mantle wedge endmember is also required for the mixing model,

121   and small changes in this value can have enormous effects on inferred CO_2 provenance.

122   A value of ~2.7 x 10^9 is usually used for the $CO_2/^3He$ ratio of the mantle wedge (e.g.

123   Hilton et al., 2002), but this value reflects the average of measurements of volatile concentrations

124   in mid-ocean ridge glasses, which show significant variation (e.g. Graham, 2002), an may not

125   represent the composition of the extensively flux-melted mantle wedge. When the $CO_2/^3He$ ratio

126   in volcanic gas samples is relatively low, the precise $CO_2/^3He$ ratio used for the mantle wedge

127   endmember becomes very important. Using data from Varekamp et al. (1992) for Sirung

128   volcano, even a 25% deviation from 2.7 x 10^9 leads to a ~10-fold change in the ratio of CO_2

129   from carbonate to CO_2 from organic C inferred from the mixing model. Therefore, results from

130   this mixing model should be used with caution, which is why we consider the simple balance

131   between the $\delta^{13}C$ of the subducting sedimentary C and the $\delta^{13}C$ of volcanic CO_2 to infer that an

132   additional ^{13}C rich reservoir external to sedimentary C is likely contributing to the arc-released

133   CO_2. We note that one of the recent studies invoking significant CO_2 contributions from

134   carbonates in the overlying crust relied almost entirely on this mixing model to argue for the

135   global importance of this CO_2 source (Mason et al., 2017). It is worth noting that both the Sunda

136 and Central American subduction margins, which this model infers to have substantial

137 contributions from crustal carbonate, are regions in which a significant amount of carbonate-rich

138 sediments are subducting.

139 Additionally, this mixing model does not permit differentiation of carbonate CO_2 source

140 (i.e. sedimentary carbonate, carbonate in altered oceanic crust, or carbonate in the overriding

141 plate) due to their indistinguishable $\delta^{13}C$ values. Likewise, our method of directly comparing the

142 $\delta^{13}C$ of subducting sediments with that of volcanic CO_2 reveals only that an additional carbonate

143 source is needed to raise the $\delta^{13}C$ of subducting C ($\sim$ -13‰) to that of arc CO_2 ($\sim$ -4 ‰). Thick

144 limestone sequences in southern Sumatra and Java have been explored as potential hydrocarbon

145 reservoirs, and because of this, they may contribute a substantial quantity of CO_2 to volcanic

146 emissions (e.g. Deegan et al., 2010). However, we find little evidence for extensive carbonate

147 deposits in northern Sumatra, particularly in the regions of greatest volcanic activity and hence

148 densest sampling (Wilson, 2002). This section of the margin also shows the greatest potential

149 for subduction of organic-rich Nicobar Fan sediments, and even if the décollement is below the

150 fan deposits as has been hypothesized (Hüpers et al., 2017), the amount of organic and inorganic

151 C subducting in sediments will be approximately equal, and an additional C source will be

152 required to balance the $\delta^{13}C$ of the sedimentary influx with that of volcanic CO_2. Carbonates in

153 the overlying crust could be a significant factor in closing the C cycling budget, but we also

154 consider carbonate in altered oceanic crust to be a likely contributor in the northern section of the

155 margin, and therefore a possible C source both throughout this margin and others.

156 Other insight, potentially significant, regarding the mixing of C from multiple sources

157 comes from study of deeply subducted metasedimentary rocks containing varying proportions of

158 C in carbonate (oxidized) and C in carbonaceous matter (reduced). Cook-Kollars et al. (2014)

159   and Kraft et al. (2017; manuscript in preparation) demonstrated extensive C isotope exchange

160   between C in the two reservoirs as they attempted equilibration particularly at the higher

161   temperatures represented in the suite. This exchange is most significant in pelite-carbonate

162   mixed rocks inferred by Cook-Kollars et al. (2014) to have experienced the most C loss by

163   decarbonation. Both the oxidized and the reduced C reservoirs were shifted in δ^{13}C from their

164   starting/oceanic compositions toward the "mantle value" of -6‰. Depending on the relative

165   abundances of carbonaceous matter and carbonate in the samples, the reduced C is shifted from

166   δ^{13}C values near -22‰ for low-grade rocks in which there is little re-equilibration with carbonate

167   near 0‰ to values as high as -8‰ at the higher grades (also see Kraft et al., 2017). Carbonate C

168   is shifted from δ^{13}C values near +1‰ for low-grade rocks in which there is little re-equilibration

169   with carbonate near 0‰ to values as low as -6‰ at the higher grades. Shift in the C isotope

170   compositions of the two subducting C reservoirs would obviously have implications for the

171   application of the three-component mixing model of Sano and Marty (1995). Yet unknown are

172   the relative degrees of C release from each of these reservoirs during the devolatilization and

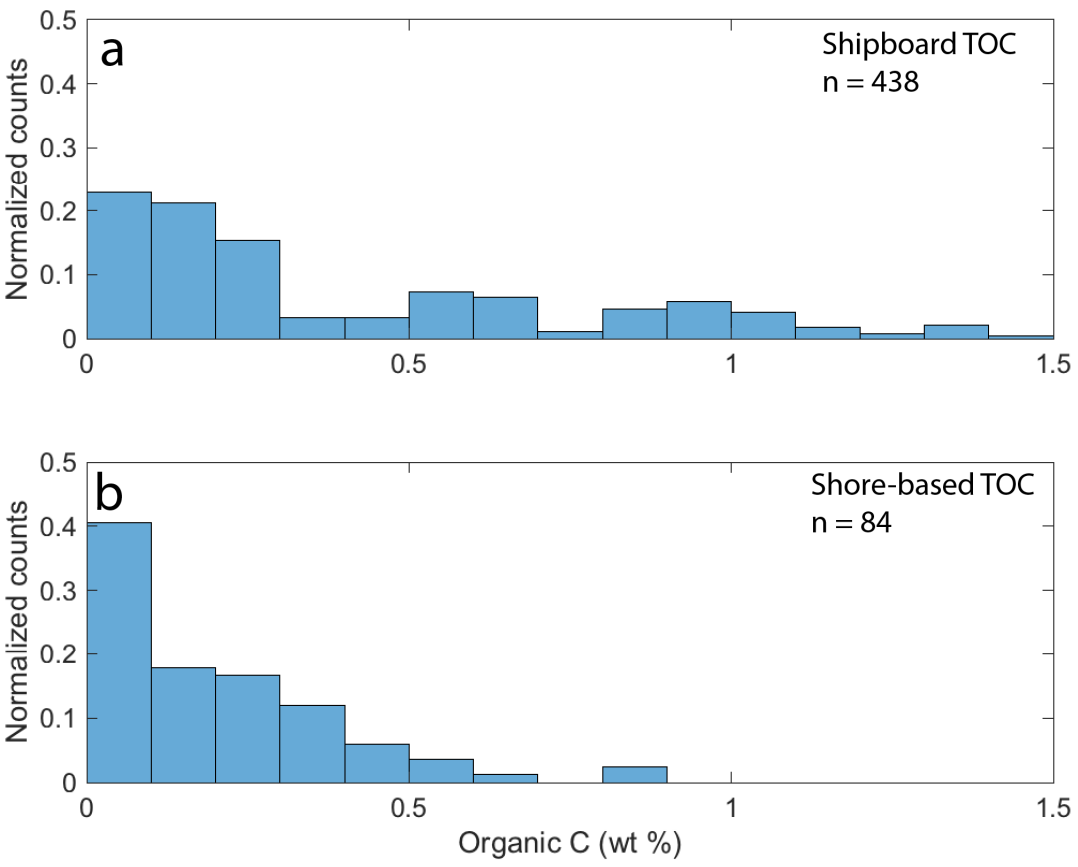173   partial melting beneath arcs at the subduction interface and in subducting slabs.

References

174 **References**

175 Argus, D.F., Gordon, R.G., and DeMets, C., 2011, Geologically current motion of 56 plates
176   relative to the no-net-rotation reference frame: Geochemistry, Geophysics, Geosystems, v.
177   12, p. n/a-n/a, doi: 10.1029/2011GC003751.
178 Bode, G., 1974, Proceedings of the Deep Sea Drilling Project, *in* Heirtzler, J., Veevers, J., and
179   Robinson, P. eds., Proceedings of the Deep Sea Drilling Project Volume 27, p. 499–502,
180   doi: doi:10.2973/dsdp.proc.27.1974.
181 Cook-Kollars, J., Bebout, G.E., Collins, N.C., Angiboust, S., and Agard, P., 2014, Subduction
182   Zone Metamorphic Pathway for Deep Carbon Cycling: I. Evidence from HP/UHP
183   Metasedimentary Rocks, Italian Alps: Chemical Geology, doi:
184   10.1016/j.chemgeo.2014.07.013.
185 Dean, S.M., McNeill, L.C., Henstock, T.J., Bull, J.M., Gulick, S.P., Austin, J.A., Bangs, N.L.,
186   Djajadihardja, Y.S., and Permana, H., 2010, Contrasting decollement and prism propoerties
187   over the Sumatra 2004-2005 earthquake rupture boundary: Science, v. 329, p. 207–210.
188 Deegan, F.M., Troll, V.R., Freda, C., Misiti, V., Chadwick, J.P., McLeod, C.L., and Davidson,
189   J.P., 2010, Magma-carbonate interaction processes and associated CO_2 release at Merapi
190   volcano, Indonesia: Insights from experimental petrology: Journal of Petrology, v. 51, p.
191   1027–1051, doi: 10.1093/petrology/egq010.
192 Expedition 22 Scientific Party, 1974, Site 211: Deep Sea Drilling Project Site Reports, v. 22, p.
193   13–36.
194 Graham, D.W., 2002, Noble gas isotope geochemistry of Mid-Ocean Ridge and Ocean Island
195   Basalts: Characterization of mantl source reservoirs, *in* Porcell, D., Ballentine, C.J., and
196   Wieler, R. eds., Noble Gases in Geochemistry and Cosmochemistry, Washington, DC,
197   Mineralogical Society of America, p. 247–318.
198 Halldórsson, S.A., Hilton, D.R., Troll, V.R., and Fischer, T.P., 2013, Resolving volatile sources
199   along the western Sunda arc, Indonesia: Chemical Geology, v. 339, p. 263–282, doi:
200   10.1016/j.chemgeo.2012.09.042.
201 Hilton, D.R., Fischer, T.P., and Marty, B., 2002, Noble gases and volatile recycling at subduction
202   zones, *in* Porcelli, D., Ballentine, C.J., and Wieler, R. eds., Noble gases in geochemistry and
203   cosmochemistry, v. 47.
204 Hüpers, A., Torres, M.E., Owari, S., McNeill, L.C., Dugan, B., Henstock, T.J., Milliken, K.L.,
205   Petronotis, K.E., Backman, J., Bourlange, S., Chemale, F., Chen, W., Colson, T.A.,
206   Frederik, M.C.G., et al., 2017, Release of mineral-bound water prior to subduction tied to
207   shallow seismogenic slip off Sumatra: Science, v. 356, doi: 10.1126/science.aal3429.
208 Kopp, H., 2013, Invited review paper: The control of subduction zone structural complexity and
209   geometry on margin segmentation and seismicity: Tectonophysics, v. 589, p. 1–16, doi:
210   10.1016/j.tecto.2012.12.037.
211 Kopp, H., Fleuh, E.R., Klaeschen, D., Bialas, J., and Reichert, C., 2001, Crustal structure of the
212   central Sunda margin at the onset of oblique subduction: Geophysical Journal International,
213   v. 147, p. 449–474.
214 Kopp, H., Flueh, E., Petersen, C., Weinrebe, W., Wittwer, A., and Scientists, M., 2006, The Java
215   margin revisited: Evidence for subduction erosion off Java: Earth and Planetary Science
216   Letters, v. 242, p. 130–142, doi: 10.1016/j.epsl.2005.11.036.
217 Kopp, H., Hindle, D., Klaeschen, D., Oncken, O., Reichert, C., and Scholl, D., 2009, Anatomy of
218   the western Java plate interface from depth-migrated seismic images: Earth and Planetary

219   Science Letters, v. 288, p. 399–407, doi: 10.1016/j.epsl.2009.09.043.

220 Kopp, H., and Kukowski, N., 2003, Backstop geometry and accretionary mechanics of the Sunda
221   margin: Tectonics, v. 22, p. n/a-n/a, doi: 10.1029/2002tc001420.

222 Kraft, K., and Bebout, G.E., 2017, Fate of subducting organic carbon: evidence from HP/UHP
223   metamorphic suites, *in* AGU Fall meeting, New Orleans.

224 Ludden, J.N., and Gradstein, F.M., 1990, Site 765: Proceedings of the Ocean Drilling Program
225   Initial Reports, v. 123, p. 63–267.

226 Lüschen, E., Müller, C., Kopp, H., Engels, M., Lutz, R., Planert, L., Shulgin, A., and
227   Djajadihardja, Y.S., 2011, Structure, evolution and tectonic activity of the eastern Sunda
228   forearc, Indonesia, from marine seismic investigations: Tectonophysics, v. 508, p. 6–21,
229   doi: 10.1016/j.tecto.2010.06.008.

230 Marty, B., Jambon, A., and Sano, Y., 1989, Helium isotopes and CO2 in volcanic gases of Japan:
231   Chemical Geology, v. 76, p. 25–40.

232 Mason, E., Edmonds, M., and Turchyn, A. V., 2017, Remobilization of crustal carbon may
233   dominate volcanic arc emissions: Science, v. 357, p. 290–294, doi:
234   10.1126/science.aan5049.

235 McNeill, L.C., Dugan, B., and Petronotis, K., 2016, Expedition 362 Scientific Prospectus:
236   International Ocean Discovery Program.

237 McNeill, L.C., Dugan, B., Petronotis, K.E., and Expedition 362 Scientists, 2017, Site U1480, *in*
238   Proceedings of the International Ocean Discovery Program, v. 362, doi:
239   10.14379/iodp.proc.362.103.2017.

240 Olivarez Lyle, A., and Lyle, M.W., 2006, Missing organic carbon in Eocene marine sediments:
241   Is metabolism the biological feedback that maintains end-member climates?
242   Paleoceanography, v. 21, doi: 10.1029/2005pa001230.

243 Pimm, A.C., 1974, Sedimentology and history of the northeastern Indian Ocean from Late
244   Cretaceous to Recent: Initial reports of the Deep Sea Drilling Project, v. 22, p. 717–803,
245   http://hdl.handle.net/10.2973/dsdp.proc.22.139.1974.

246 Planert, L., Kopp, H., Lueschen, E., Mueller, C., Flueh, E.R., Shulgin, A., Djajadihardja, Y., and
247   Krabbenhoeft, A., 2010, Lower plate structure and upper plate deformational segmentation
248   at the Sunda-Banda arc transition, Indonesia: Journal of Geophysical Research, v. 115, doi:
249   10.1029/2009jb006713.

250 Plank, T., and Ludden, J.N., 1992, Geochemistry of sediments in the Argo Abyssal Plain at site
251   765: A continental margin reference section for sediment related recycling in subduction
252   zones: Proceedings of the Ocean Drilling Program, Scientific Results, v. 123, p. 167–189.

253 Sano, Y., and Marty, B., 1995, Origin of carbon in fumarolic gas from island arcs: Chemical
254   Geology, v. 119, p. 265–274.

255 Varekamp, J.C., Kreulen, R., Poorter, R.P.E., and van Bergen, M.J., 1992, Carbon sources in arc
256   volcanism, with implications for the carbon cycle: Terra Nova, v. 4.

257 Wilson, M.E.J., 2002, Cenozoic carbonates in Southeast Asia: Implications for equatorial
258   carbonate development: Sedimentary Geology, v. 147, p. 295–428, doi: 10.1016/S0037-
259   0738(01)00228-7.

260

261

262

263   Supplemental figures
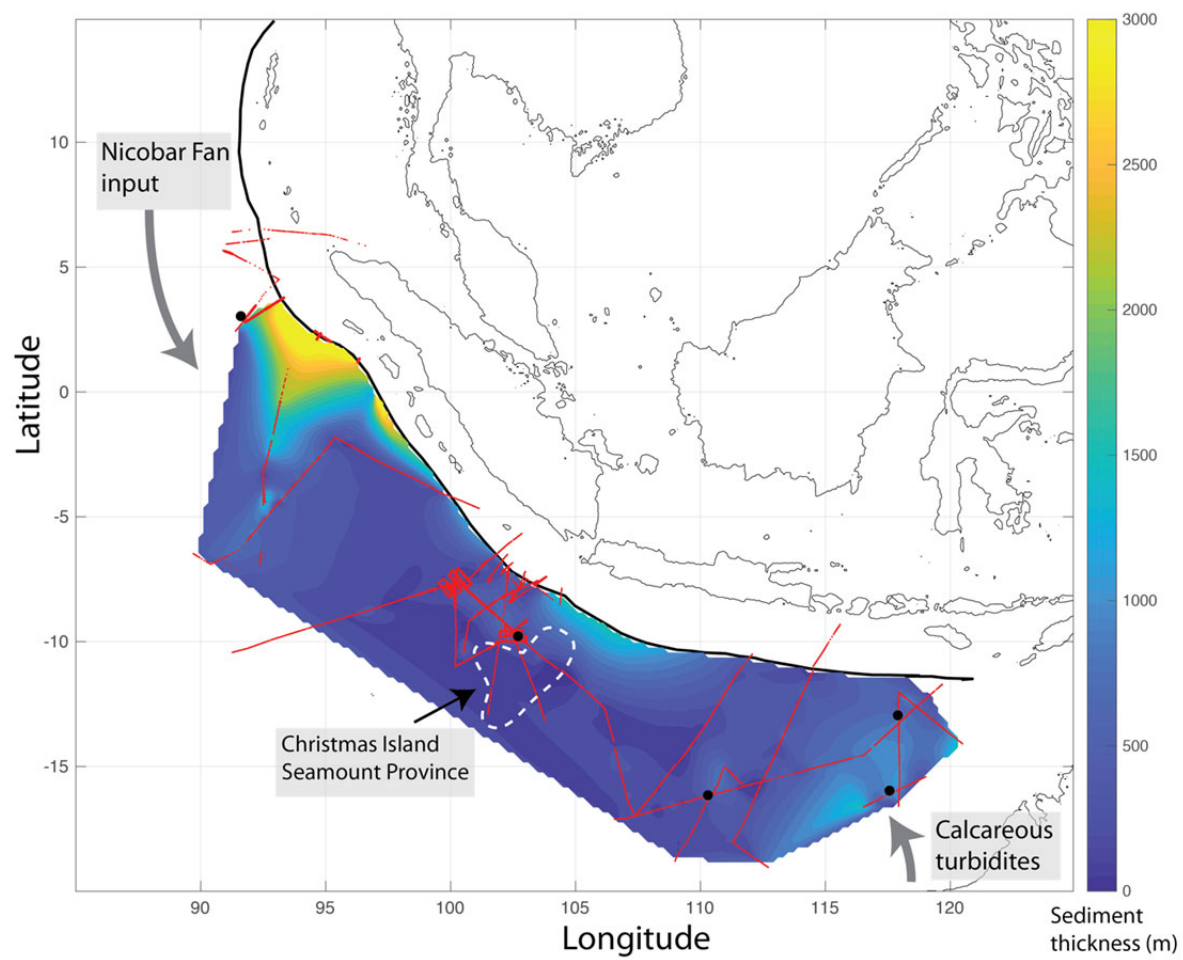
264   Figure DR1

265

266

267

268

269   Figure DR2
270

271

276

277   Figure captions

278

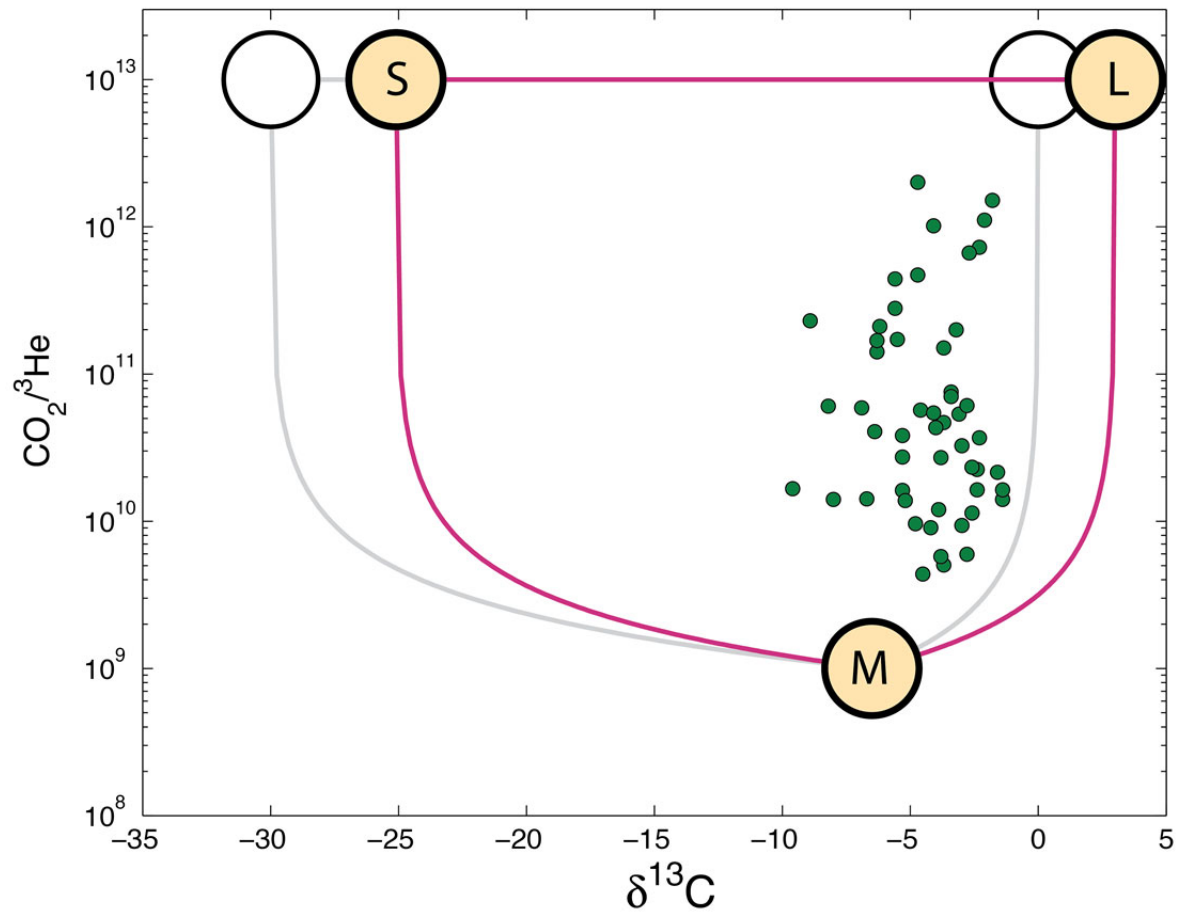279   Figure DR1. Histograms showing distributions of shipboard (a) and shore-based (b) Total

280   Organic Carbon (TOC) measurements generated for this study from DSDP 211, 213, 260, 261,

281   262 and ODP 765. Normalized counts represent the fraction of samples that fall within a given

282   range of TOC values. Shipboard values are calculated as the difference between total C,

283   measured by combustion elemental analysis, and carbonate C, measured by coulometry whereas

284   shore-based values represent direct measurements of TOC following acidification to remove

285   carbonate phases. While we were not able to analyze splits of precisely the same samples used

286   for shipboard analyses, the pronounced difference in the distributions and number of data points

287   strongly suggests that shipboard analyses overestimate the true TOC. Indeed, we were unable to

288   reproduce TOC values over 0.86 wt% C with shore-based analyses.

289

290   Figure DR2. Model of overall sediment thickness model based on seismic picks (small red

291   points) of seafloor and acoustic basement depth. Points outside the interpolated region represent

292   regions where acoustic basement was not reliably imaged and picks could only be made to

293   constrain unit thicknesses. Black points indicate the DSDP/ODP/IODP sites that are labeled in

294   Fig. 1. The color scale saturates at 3 km sediment thickness. Material from the Nicobar Fan (to

295   the northwest) and calcareous turbidites from the Australian margin (to the southeast) are

296   separated by the Christmas Island Seamount Province.

297

298

299   Figure DR3. The three-endmember mixing model of Sano and Marty (1995) can be used to infer

300   the provenance of volcanic CO_2 from measured $\delta^{13}C$ and $CO_2/^3He$ ratios in volcanic gases

301   (Halldórsson et al., 2013; Varekamp et al., 1992). Solving a set of linear equations for the

302   fraction of CO_2 from sedimentary carbonate (termed "limestone" in the original reference and

303   represented the L endmember), organic C (termed "sedimentary" and denoted by S), and mantle

304   wedge (M) sources. Open, unshaded circles represent global averages for the S and L

305   endmembers that were used previously, and yellow circles represent values measured for this

306   study. The $CO_2/^3He$ ratio of the mantle wedge is inferred from measurements of Mid-Ocean

307   Ridge Basalt (MORB), but whether these values accurately represent the mantle wedge

308   composition is unclear. For some volcanoes, the results of this mixing model are exceedingly

309   sensitive to the exact $CO_2/^3He$ used.

Table DR1. Concentrations and isotopic compositions of carbonate and organic C

2019180_Table DR1.xlsx